PB84-142314

Evaluation of Several Numerical Advection Schemes

(U.S.) Environmental Sciences Research Lab.
Research Triangle Park, NC

1983

U.S. Department of Commerce
National Technical Information Service
NTIS

TECHNICAL REPORT DATA
(Please read Instructions on the reverse before comp)

1. REPORT NO.	2.	PB84-142314
EPA-600/J-83-142		

4. TITLE AND SUBTITLE	5. REPORT DATE
AN EVALUATION OF SEVERAL NUMERICAL ADVECTION SCHEMES (Journal Version)	1983
	6. PERFORMING ORGANIZATION CODE
7. AUTHOR(S)	8. PERFORMING ORGANIZATION REPORT NO.
K.L. Schere	
9. PERFORMING ORGANIZATION NAME AND ADDRESS	10. PROGRAM ELEMENT NO.
Same as box 12	CDWA1A/01-1332 (FY-83)
	11. CONTRACT/GRANT NO.
12. SPONSORING AGENCY NAME AND ADDRESS	13. TYPE OF REPORT AND PERIOD COVERED
ENVIRONMENTAL SCIENCES RESEARCH LABORATORY--RTP,NC OFFICE OF RESEARCH AND DEVELOPMENT U.S. ENVIRONMENTAL PROTECTION AGENCY RESEARCH TRIANGLE PARK, NORTH CAROLINA 27711	In-house
	14. SPONSORING AGENCY CODE
	EPA/600/09

15. SUPPLEMENTARY NOTES

REF: Atmospheric Environment, 17(10):1897-1907, 1983

16. ABSTRACT

Three categories of numerical advection techniques are tested: SHASTA, a flux-corrected one-dimensional algorithm; FCT, a multi-dimensional flux-corrected technique; and the BIQUINTIC method, a polynomial approximation algorithm. The tests include the transport of a finite amount of material through a 25 x 25 cell grid driven by three different flow fields: one-dimensional linear flow, two-dimensional linear flow, and rotational flow. For each of these tests, two intial distributions of material are used: a rectangular block-shape and an ellipse-shape. In addition, a test with a non-divergent flow field with a homogeneous material field was performed to check for inherent divergence in a partcular method. Results show that the FCT and BIQUINTIC methods maintain the integrity of an initial distribution of material better than SHASTA through a simulation. While SHASTA is the fastest of the methods tested computationally it also produces the greatest amount of spurious numerical diffusion. The FCT method has a tendency to flatten the top of a peaked distribution, and the BIQUINTIC method tends to produce a peak in a top-hat distribution during numerical transport. The BIQUINTIC scheme requires more computer time to execute than the other methods tested.

17. KEY WORDS AND DOCUMENT ANALYSIS

a. DESCRIPTORS	b. IDENTIFIERS/OPEN ENDED TERMS	c. COSATI Field/Group

18. DISTRIBUTION STATEMENT	19. SECURITY CLASS *(This Report)*	21. NO. OF PAGES
RELEASE TO PUBLIC	UNCLASSIFIED	12
	20. SECURITY CLASS *(This page)*	22. PRICE
	UNCLASSIFIED	

EPA Form 2220-1 (9-73)

REPRODUCED BY
NATIONAL TECHNICAL
INFORMATION SERVICE
U.S. DEPARTMENT OF COMMERCE
SPRINGFIELD, VA. 22161

EPA-600/J-83-142
JOURNAL ARTICLE

Atmospheric Environment Vol. 17, No. 10, pp. 1897–1907, 1983
Printed in Great Britain.

0004-6981/83 $3.00 + 0.00
Pergamon Press Ltd.

AN EVALUATION OF SEVERAL NUMERICAL ADVECTION SCHEMES

KENNETH L. SCHERE*

Meteorology and Assessment Division, Environmental Sciences Research Laboratory, Research Triangle Park, NC 27711, U.S.A.

(*First received* 28 *February* 1982 *and received for publication* 27 *April* 1983)

Abstract—Three categories of numerical advection techniques are tested: SHASTA, a flux-corrected one-dimensional algorithm; FCT, a multi-dimensional flux-corrected technique; and the BIQUINTIC method, a polynomial approximation algorithm. The tests include the transport of a finite amount of material through a 25×25 cell grid driven by three different flow fields: one-dimensional linear flow, two-dimensional linear flow, and rotational flow. For each of these tests, two initial distributions of material are used: a rectangular block-shape and an ellipse-shape. In addition, a test with a non-divergent flow field with a homogeneous material field was performed to check for inherent divergence in a particular method. Results show that the FCT and BIQUINTIC methods maintain the integrity of an initial distribution of material better than SHASTA through a simulation. While SHASTA is the fastest of the methods tested computationally it also produces the greatest amount of spurious numerical diffusion. The FCT method has a tendency to flatten the top of a peaked distribution, and the BIQUINTIC method tends to produce a peak in a top-hat distribution during numerical transport. The BIQUINTIC scheme requires more computer time to execute than the other methods tested.

1. INTRODUCTION

The evolving class of air quality simulation models (AQSM) is becoming a useful resource for air quality analysts, meteorologists, engineers and others involved in urban and regional air pollution control. These models solve a numerical approximation to the advection–diffusion equation with the addition of source emissions, sink terms and often a set of chemical reaction terms. Most solution methods applied to these AQSM's make use of the fractional step method of Yanenko (1971) that allows for separate successive solutions of the various component-processes. Certainly one of the most central of these components is the advection step. This involves solving a numerical approximation to the advective transport equation that can be written in two-dimensional (2-D) form as

$$\frac{\partial c}{\partial t} = -\frac{\partial (uc)}{\partial x} - \frac{\partial (vc)}{\partial y}, \qquad (1)$$

where c is the concentration of a particular pollutant species and u and v are the wind components in the x and y directions, respectively. Equation (1) expresses the conservation of mass of the species whose concentration is c. Credible model results require the efficient and accurate solution of this equation in the advective model component. The work described here is an attempt to evaluate several numerical methods for the solution of the advection equation that also appear practical for integration into the structure of an AQSM.

The impetus for this study developed from tests performed on the Urban Airshed Model, a three-dimensional (3-D) Eulerian grid photochemical AQSM developed by Systems Applications, Inc. (Reynolds and Roth, 1983; Reynolds *et al.*, 1973). While investigating the various components of the model it was found that the numerical advection algorithm used, a non-mass-conservative version of SHASTA (Killus *et al.*, 1977; Boris and Book, 1973, 1976) produced an unacceptably large amount of artificial, or numerical diffusion when subjected to independent advection tests. The implications of this result for air quality modeling studies are potentially serious. Numerical diffusion within finite-difference solution schemes to the advection equation can mask the effects of real atmospheric diffusion, also numerically simulated in an AQSM, as well as seriously deflate the peak concentration values within the model domain. These values are of prime interest to the air quality analyst. It is clear that numerical diffusion cannot totally be eliminated from a finite-difference solution scheme for the advection equation as it helps to insure computational stability in the solution. However, the optimum method needed for air quality modeling work is one that minimizes artificial diffusion while maintaining the integrity of the concentration field being advected. Computer considerations such as execution time must also be made in the final choice of a method.

Because of the wide and varying applications of AQSM's the numerical advection schemes studied here are modular in nature, relatively easy to implement, and not extremely sensitive to variations in boundary or initial conditions. Most are variations of the flux-corrected transport method first proposed by Boris and

* On assignment from the National Oceanic and Atmospheric Administration, U.S. Department of Commerce.

AE - 17:10 - C

Book (1973) and later generalized by Zalesak (1979). Also considered is a new scheme based on a biquintic polynomial and developed by Lamb (1983) for use in a regional scale AQSM. The tests described involve the advection of an element of mass through a 25 × 25 cell 2-D grid. In one case the mass element has a rectangular block-shape and in the other it is a shape with elliptical cross-sections. Tests were performed with three different flow fields for advection: one-dimensional (1-D) linear flow, 2-D linear flow and rotational flow. In addition, a test with a constant mass field and an analytically non-divergent flow field was included as a check for convergence zones in the solution.

2. NUMERICAL SOLUTION METHODS

Five methods for solving numerical advection problems are tested here. Four of them are variations on the flux-corrected transport approach and one involves a polynomial fit to the transport field. All are based on finite-difference approximations to the solution of Equation (1). A leap-frog time step procedure is often used in solutions of finite-difference transport problems of this type because of its associated stability and absence of damping effects. However, the maintenance of three time levels is required for this centered-in-time method and most large AQSM's cannot afford the luxury of the computer storage requirements for three levels. Therefore, we use variations of forward time differencing for the tests presented here along with centered-in-space differences being careful to maintain the Courant condition for numerical stability (Roache, 1972). This is also the method most often used in numerical AQSM's. Since the flow fields used in all tests here are constant in time, a fixed time step can be employed. In a real atmospheric simulation where flow fields vary in time, the time step typically varies during the solution such that the Courant condition is maintained.

SHASTA

A general category of numerical advection methods was developed over the last decade that solved some of the persistent problems associated with transport schemes prior to this period (Boris and Book, 1973, 1976; Book *et al.*, 1975). This is the category of flux-corrected transport methods. The original 1-D element in this category is SHASTA (sharp and smooth transport algorithm). It is a synthesis of a higher-order and a lower-order scheme for numerically integrating Equation (1). By itself, a higher order (2 and above) finite-difference method is more accurate than a low-order method but is prone to develop dispersive 'ripples' in the solution, particularly in an area of steep gradients. Lower-order schemes, such as the donor cell method (Gentry *et al.*, 1966), will not develop ripples in the solution, but tend to generate large amounts of numerical diffusion, which can wreck havoc in an air quality simulation with large concentration gradients. SHASTA computes a net flux as a weighted average of a flux calculated from a low order scheme and a flux from a high order scheme in a fashion that insures that the high order flux is weighted as heavily as possible without introducing ripples. The weighting procedure is known as 'flux-correction'.

The step-by-step procedure for the 1-D algorithm, as outlined by Zalesak (1979), proceeds as follows:

(1) Compute $F^{L}_{i+(1/2)}$, the transportive flux between spatial grid points i and $i+1$ given by a low-order scheme.
(2) Compute $F^{H}_{i+(1/2)}$, the transportive flux given by a high order scheme.
(3) Define the 'anti-diffusive flux':

$$A_{i+(1/2)} \equiv F^{H}_{i+(1/2)} - F^{L}_{i+(1/2)}.$$

(4) Compute the intermediate (*) new time level solution:

$$c_i^{(n+1)*} = c_i^n - \Delta x_i^{-1}\left[F^{L}_{i+(1/2)} - F^{L}_{i-(1/2)}\right],$$

where c_i^n is the transported quantity (concentration of pollutant species, for example), at time n and grid point i, and Δx_i is the distance between adjacent grid points on a regularly spaced mesh.
(5) 'Limit' the $A_{i+(1/2)}$ such that c^{n+1} as computed in step 6 below is free of extreme values not found in c^n or $c^{(n+1)*}$:

$$A^{LIM}_{i+(1/2)} = L_{i+(1/2)} A_{i+(1/2)},$$
$$0 \leqslant L_{i+(1/2)} \leqslant 1.$$

(6) Apply the limited anti-diffusive fluxes:

$$c_i^{n+1} = c_i^{(n+1)*} - \Delta x_i^{-1} \times \left[A^{LIM}_{i+(1/2)} - A^{LIM}_{i-(1/2)}\right].$$

Details of the flux-correction (step 5) can be found in Boris and Book (1973) or Zalesak (1979).

The version of the SHASTA algorithm used in the Urban Airshed AQSM omits step 5 from the above procedure. This is described as the non-flux-limited, non-mass-conservative version of SHASTA by Killus *et al.* (1977). In the tests presented in this work it is referred to as SHASTA-1. In addition, the original algorithm of Boris and Book (1973) that includes the flux-correction, step 5, is referred to as SHASTA-2 in the tests.

The advection tests performed for this study were made on a 2-D grid while the SHASTA technique is 1-D. This apparent inconsistency is resolved by a procedure known as time-splitting, identical to the fractional-step method mentioned earlier. The advection is done first in the x-component direction, and then separately in the y-component direction on the initial time step. In the following time step the order is reversed, and so on through the simulation.

SHASTA requires a single boundary condition grid cell at each end of the string of computational cells. For outflow at the boundary, the value of the boundary cell was set to the existing value in the adjacent compu-

tational cell. For inflow, the value of the boundary condition at the end of the previous time step was used.

FCT

Zalesak (1979) extended the concept of flux-corrected transport (FCT) to any number of dimensions in a simple, generalized format. The procedure for the multi-dimensional FCT follows along the lines of the six steps outlined for the SHASTA method, except that for each step other component terms are added for each dimension beyond the first. The advantage of the generalized format of FCT is that time-splitting becomes unnecessary, as numerical transport proceeds in all dimensions (2 for the tests in this study) simultaneously. While this is not necessarily more computationally efficient there are many problems where time-splitting produces unacceptable numerical results, such as those involving incompressible or nearly compressible flow fields (Zalesak, 1979).

The implementation of this generalized FCT scheme for our 2-D tests differs slightly from the original formulation. Zalesak used leapfrog time differencing and a low-order flux calculation based on the donor cell method plus a zeroth-order diffusive flux with coefficient 1/8. We use forward-time differencing for reasons stated above and have dropped the zeroth-order diffusive flux term. Two versions of the high-order flux computation are tested. In one, an eighth-order spatially accurate form is used (FCT8) and in the other, a fourth-order form (FCT4) is used.

For FCT8, four boundary cells are required at each edge of a row or column of the computational domain and two boundary cells are necessary for FCT4. The values in these cells are set in a fashion similar to that described for SHASTA, except that the values for the first boundary cell are also assigned identically to the remaining cells extending outward in the row or column.

BIQUINTIC

During the development stage of a regional scale (1000 km) photochemical AQSM (Lamb, 1983), it was reasoned that for purposes of accuracy and efficiency in the new model the existing numerical advection techniques all had serious drawbacks. Most seemed to have problems representing large concentration gradients in the advected field. On the regional scale, large pollutant concentration gradients both in the vertical and the horizontal are not uncommon. Also the size of the computational mesh in the proposed model was large enough that it precluded the concurrent residence in computer core storage of all the necessary variables for advection on most large contemporary machines. Most existing advection methods required the entire grid to be resident in storage at one time. For these reasons and others, a new form of numerical advection algorithm was conceived and developed by Lamb that would circumvent the obstacles toward numerical advection in a regional AQSM.

The resulting algorithm performs both advection and diffusion in one step. The description of the concentration field at any time t_{n+1}, for species i, has the form

$$c_i(x, y, t_{n+1}) = \int\int_{-\infty}^{\infty} c_i(x', y', t_n) \times p(x, y, t_{n+1} | x', y', t_n)\, dx'\, dy' \quad (2)$$

where p is the Green's function of the advection–diffusion equation for c_i. In order to evaluate this expression, $c_i(t_n)$ must be expressed as a continuous, rather than a discrete, function. Using polynomials to represent the discrete set of $c_i(t_n)$ values, the integrals that result from Equation (2) can be evaluated analytically to give algebraic expressions for $c_i(t_{n+1})$ at each grid point (x, y).

Instead of expressing the polynomials about (x, y) for $c_i(t_n)$ they are, in practice, developed around $(\hat{x}, \hat{y})$ for $c_i(t_n)$, where the latter point is the location of the Green's function maximum in the neighborhood of (x, y). If the space variables (x, y) are transformed to a new set of variables (η, ζ), expressing the relationship between (x, y) and $(\hat{x}, \hat{y})$, then an explicit equation may be developed for $c_i(\eta, \zeta, t_{n+1})$

$$c(\eta, \zeta, t_{n+1}) = \sum_{i=0}^{k} \sum_{j=0}^{k} A_{ij} \eta^i \zeta^i, \quad (3)$$

where the coefficients A_{ij} can be determined using a Lagrangian interpolating polynomial and k is the maximum order of the terms in the expansion of Equation (3). Lamb developed the 2-D relationships for $k = 2$ (biquadratic), $k = 3$ (bicubic) and $k = 5$ (biquintic) and tested the latter two for possible inclusion in the regional AQSM.

Of particular interest is the fact that if $(\hat{x}, \hat{y}) \equiv (x, y)$ and $k = 2$, the 1-D formulation collapses to the well known Lax–Wendroff finite difference approximation of the advection equation. That scheme, however, is computationally stable only if the Courant condition is satisfied. The class of algorithms developed by Lamb is unconditionally stable. This becomes greatly advantageous in a multi-day simulation with a regional AQSM where a large time step is a virtual necessity. Also, the computer core requirements of each of these algorithms is independent of the size of the modeling region or the number of dependent variables, since a selected portion of the computational grid may be isolated for solution at any one time. For a complete description of the derivation of these techniques and examples of their application to test problems the interested reader is referred to Lamb (1983) and Lamb and Mitchell (1983).

For the tests performed in this study only the biquintic form of this class of techniques was selected. Initial tests by the developers showed that while it had the longest computation times, it was also the most accurate. There are three boundary cells that must be assigned values at each end of a row or column in the grid for the BIQUINTIC algorithm. This is handled in

a manner similar to that described for the FCT methods.

3. ADVECTION TESTS

Each of the numerical solution techniques described above for the advection equation was employed in several advection experiments designed to elicit both the strengths and shortcomings of the methods. One of the most severe tests in this regard is that of transporting a field containing a large gradient of material. Three of the four tests described below are variations of this test. A test involving small or no material gradients transported by a well-behaved flow field would not discriminate clearly among the techniques tested. The final test involves a constant mass field with a more complex flow field.

The computational grid used in all tests is a 25×25 cell mesh. Because the incentive for this work was based on air quality simulation modeling we will follow through the tests with the parameter names and dimensions borrowed from that application. Therefore, each cell is assumed to measure 4 km on a side and the material being transported through the mesh may be viewed as a mass of non-reactive air pollutant whose concentration is expressed in arbitrary units. The flow field also becomes a wind field. Figure 1 displays the four wind fields used in the advection tests.

The wind field for the 1st test, shown in Fig. 1(a), consists of simple constant 1-D linear flow of $2.22\,\mathrm{m\,s^{-1}}$, or 2 grid cells $\mathrm{h^{-1}}$. The initial mass concentration in tests with this flow field is located near the top center section of the grid. Figure 1(b) shows a constant 2-D linear wind field with a velocity of $2.22\,\mathrm{m\,s^{-1}}$ in each coordinate direction. For this case the initial mass concentration is located near the top left corner of the grid. The 3rd test, a rotational flow field, is pictured in Fig. 1(c). The rotation is counterclockwise about the center of the grid at a constant

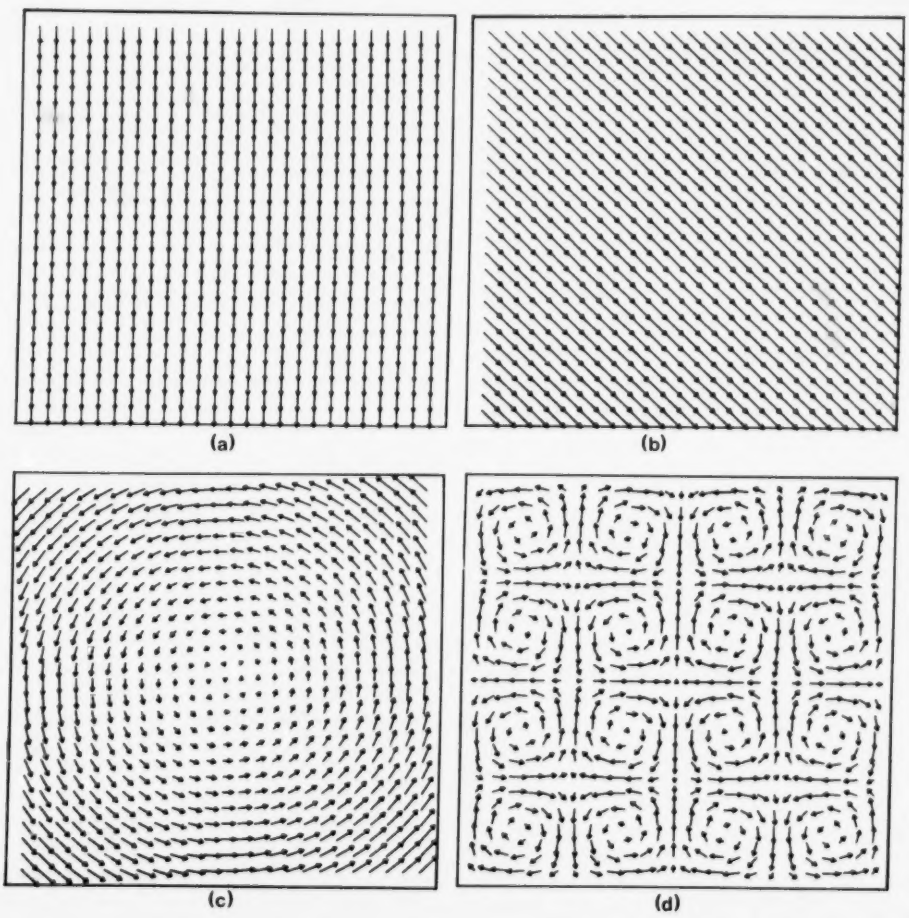

Fig. 1. Wind flow fields used in the numerical advection tests including (a) 1-D linear flow, (b) 2-D linear flow, (c) rotational flow and (d) non-divergent flow.

angular velocity of $0.08\ \pi\ h^{-1}$. At this rate of rotation wind velocities vary radially outward from the center of the grid from 0.0 to 3.4 m s^{-1} near the edges. The initial mass concentration for the rotational test is located near the top center part of the grid. The final test uses an analytically non-divergent wind field, shown in Fig. 1(d). This test, initialized with a mass field of constant concentrations, indicates whether a numerical advection technique possesses anomalous sources or sinks of mass. The expressions for the u and v wind components for this flow field are

$$u = -4\sin\left(\frac{I-13}{2}\right)\cos\left(\frac{J-13}{2}\right)$$

$$v = 4\sin\left(\frac{J-13}{2}\right)\cos\left(\frac{I-13}{2}\right), \tag{4}$$

where u and v are expressed in m s^{-1} and I and J are the x- and y- direction grid cell numbers, respectively, beginning with (1, 1) in the lower left corner of the grid. At any grid location the 2-D non-divergence property should hold, or

$$\frac{\partial u}{\partial x} + \frac{\partial v}{\partial y} = 0, \tag{5}$$

and the mass distribution in the grid should remain temporally and spatially constant.

Two different initial mass distributions were used in the first three advection tests described to test for differences in the preservation of symmetry among the various transport algorithms. The two initial distributions are shown in Fig. 2. The rectangular, or block-shaped, mass distribution, in Fig. 2(a), is 5×5 mesh points in size, each at a concentration of 100 units. The spheroid-shaped mass distribution with elliptical vertical cross-sections in the x- and y- directions is displayed in Fig. 2(b). Its peak at the center is 100 units and the concentration decreases to 0 at 5 mesh points from the peak along the major axis and 3 along the minor axis. For simulation, the distribution is initially oriented with the major axis in the direction of transport. For the non-divergence test, the mass field is initialized at 100 units in each cell.

To summarize, five numerical advection methods were tested with three flow fields initialized with two different mass distributions and one flow field with a single mass distribution, leading to 35 individual tests. They are summarized in the matrix given in Table 1. In all cases a numerical time step of 5 min was used and the Courant number in the tests varied from 0.0 to 0.3 at a maximum. The computer simulations were performed on a UNIVAC 1100/82 system using standard FORTRAN programming techniques for all algorithms.

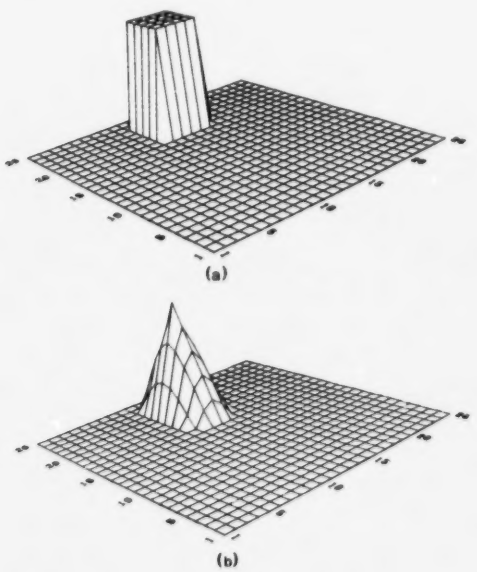

Fig. 2. The initial mass distributions used in the numerical advection tests including (a) block-shaped mass and (b) ellipse-shaped mass. The peak concentration of each distribution is 100 units.

Table 1. Matrix of numerical advection experiments

Algorithm	Flow-type / Mass-shape	1-D Linear Block	1-D Linear Ellipse	2-D Linear Block	2-D Linear Ellipse	Rotation Block	Rotation Ellipse	Non-Divergence
FCT8		X	X	X	X	X	X	X
FCT4		X	X	X	X	X	X	X
SHASTA-1		X	X	X	X	X	X	X
SHASTA-2		X	X	X	X	X	X	X
BIQUINTIC		X	X	X	X	X	X	X

4. RESULTS

Comparisons of the simulated mass fields were made with the exact solutions at selected points in time. Plots of the mass fields were made in 3-D to study the relative amounts of distortion from the original mass distribution and the amount of numerical diffusion occurring during the simulation. Also, several parameters of interest were computed that help to determine the accuracy of the solution technique (Chock and Dunker, 1983):

$$\text{Mass Conservation Ratio} = \Sigma c(t)/\Sigma c(0) \quad (6)$$

$$\text{Mass Distribution Ratio} = \Sigma c^2(t)/\Sigma c^2(0) \quad (7)$$

$$\text{Average Absolute Error} = \Sigma |c(t) - c_e(t)|/(25)^2 \quad (8)$$

$$\text{Maximum Absolute Error} = \max|c(t) - c_e(t)|, \quad (9)$$

where $c(t)$ and $c(0)$ are the simulated concentrations at a particular grid cell at time t and at the start, respectively; $c_e(t)$ is the exact solution at time t; and all summations are performed over the entire grid.

The mass distribution ratio is affected by the mass spreading into areas of the grid that should remain free of mass, by damping of the peak concentrations, by negative ripples, or by diffusive effects in the solution.

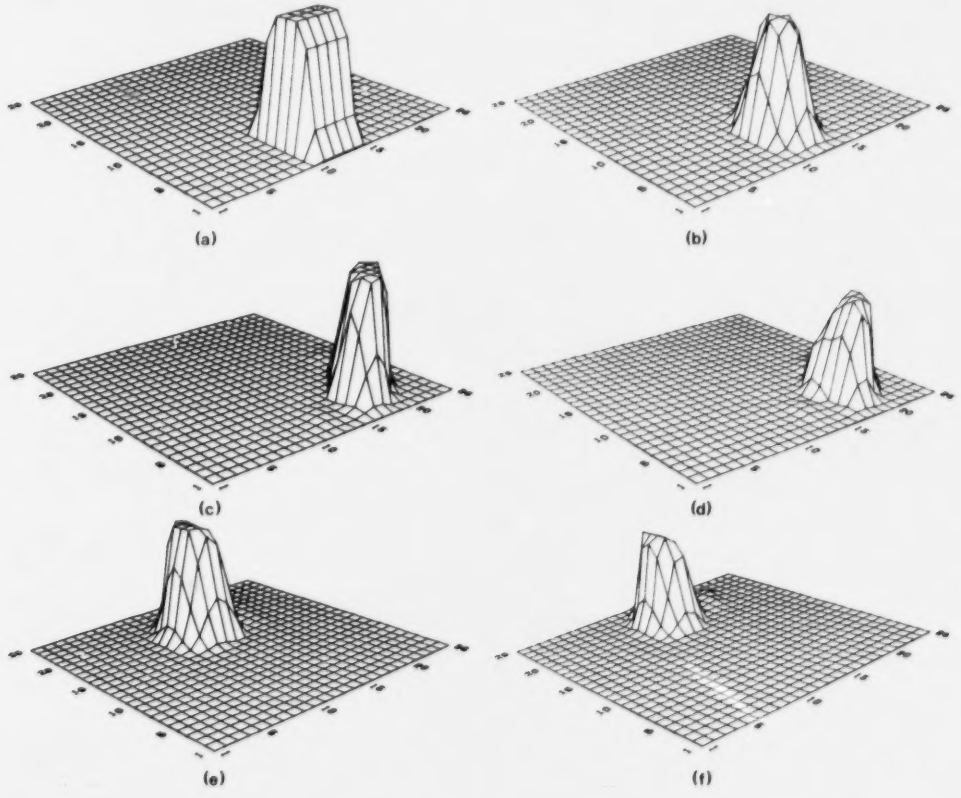

Fig. 3. Concentration fields of mass resulting from tests of the FCT4 algorithm with (a) 1-D linear flow, block-shape initial mass, after 96 time steps, (b) 1-D linear flow, ellipse-shape initial mass, after 84 time steps, (c) 2-D linear flow, block-shape initial mass, after 96 time steps, (d) 2-D linear flow, ellipse-shape initial mass, after 84 time steps, (e) rotational flow, block-shape initial mass, after 300 time steps and (f) rotational flow, ellipse-shape initial mass, after 300 time steps.

While any one technique may be perfectly mass-conserving it may also have a poor mass distribution ratio. The average absolute error is a measure of the average distortion in the mass field, and the maximum absolute error is sensitive to the damping and displacement of the peak.

Only a brief comment will be made here on the mass conservation ratio for the tests performed. All methods tested conserved mass fairly well during the simulations. The FCT methods were found to conserve mass within 0.2% in the linear tests and 5.5% in two revolutions in the rotational tests. Mass conservation departures in the SHASTA tests were no more than 1.3% in the linear tests and 7.9% in the rotational, and for the BIQUINTIC tests, mass conservation departures were no more than 8% in the linear tests and 23.9% in the rotational. The BIQUINTIC algorithm's relatively poor mass conservation performance in the rotational tests is due largely to the method's sensitivity to the flow trajectory determination. For the rotational tests a linearized approximation to the curved flow field was used (Fig. 1c). Had the flow field been approximated by curvilinear or arc segments, the mass deviation in the rotational tests would have been greatly reduced.

The non-divergent flow test did not show much variation among the advection algorithms. After 60 time steps of transport with the flow field shown in Fig. 1(d), the FCT and BIQUINTIC methods showed mass fields identical to the initial state, with concentration values of 100 in each cell. Tests with the SHASTA methods revealed periodic concentration fluctuations of a few percent in the grid; however, these fluctuations did not indicate serious convergence or divergence zones in the solution. For the methods tested here, the artificial convergence of mass in the numerical solution does not appear to be a problem.

The remaining tests involve the advection of a mass element initially contained in a group of neighboring cells through a grid otherwise composed of cells with no mass. Figures 3, 4 and 5 depict 3-D views of the concentration fields in the tests after a period of time has elapsed. Figure 3 contains results from one of the FCT algorithms, FCT4; Fig. 4 contains results from one of the SHASTA methods, SHASTA-2; and Fig. 5 displays results from the BIQUINTIC method. In each of the figures, the a, c and e components represent advection of the block-shaped mass that has an initial distribution shown in Fig. 2(a). The b, d and f components are results from advection of the elliptical-shaped mass with an initial distribution given in Fig. 2(b). For the 1-D and 2-D linear tests, results shown are after 96 time steps for the block-shape (a and c) and 84 time steps for the ellipse-shape (b and d);

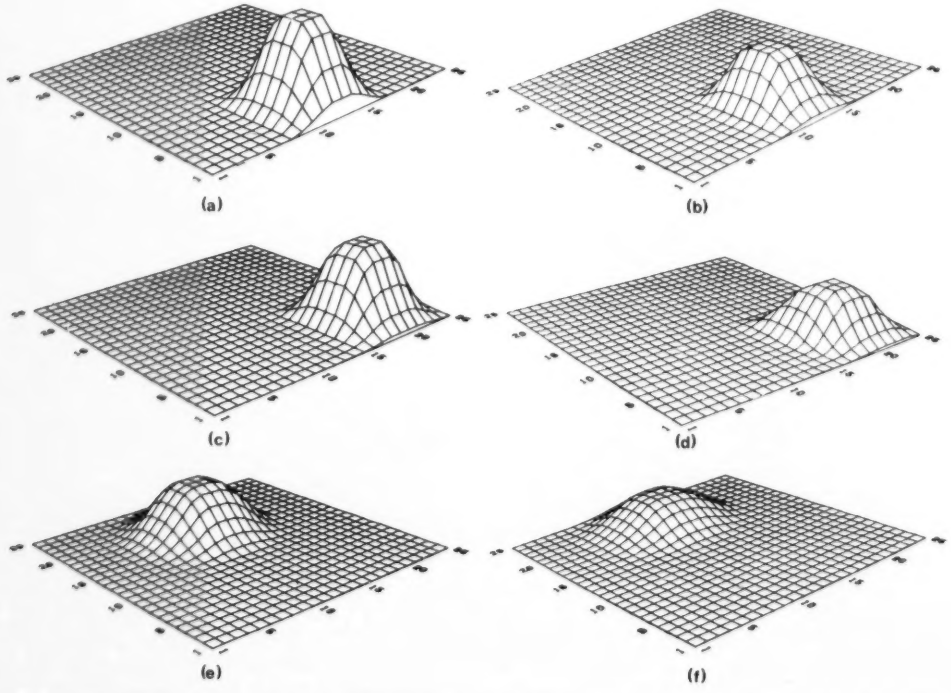

Fig. 4. Concentration fields of mass resulting from tests of the SHASTA-2 algorithm with (a) 1-D linear flow, block-shape initial mass, after 96 time steps, (b) 1-D linear flow, ellipse-shape initial mass, after 84 time steps, (c) 2-D linear flow, block-shape initial mass, after 96 time steps, (d) 2-D linear flow, ellipse-shape initial mass, after 84 time steps, (e) rotational flow, block-shape initial mass, after 300 time steps and (f) rotational flow, ellipse-shape initial mass, after 300 time steps.

and for the rotational tests, the results shown are after 1 complete revolution, or 300 time steps (e and f).

For the 1-D linear test the deformation in the original mass shape is largely in the direction of transport for the FCT4 and BIQUINTIC cases but is nearly equal in the transport and cross-transport directions for SHASTA-2. Curiously, the final mass shape in the 1-D tests of the ellipse-shape appears more block-like with the FCT4 algorithm (3b), and the resulting distribution for the block-shape advected by the BIQUINTIC method is peaked (5a). These deformation trends do not occur with a transport of the block-shape by FCT4 (3a) or transport of the ellipse-shape by BIQUINTIC (5b), where the shapes of the original distributions are preserved better during advection. This suggests that the FCT4 and BIQUINTIC algorithms have a preferential mass distribution for advection of a block- and ellipse-shape, respectively. The magnitude of the peak for these two algorithms has been maintained quite well in the tests, although some negative rippling has occurred in the wake of the BIQUINTIC trajectory (5a and b). The results in the SHASTA-2 1-D tests (4a and b) show the peak concentration of the mass to be severely damped and considerable numerical diffusion to have occurred. The ellipse-shape (4b) has become more 'blocked' after advection by SHASTA-2. It would appear that while the flux-correction techniques do not produce negative ripples they tend to force the mass distribution to become blocked.

Similar effects are seen in the results of the 2-D linear tests although the distortion of the original shapes are greater after advection. The FCT4 results (3c and d) are particularly distorted although vertical cross-sections through the resulting masses still approach the correct distribution. The BIQUINTIC results (5c and d) are

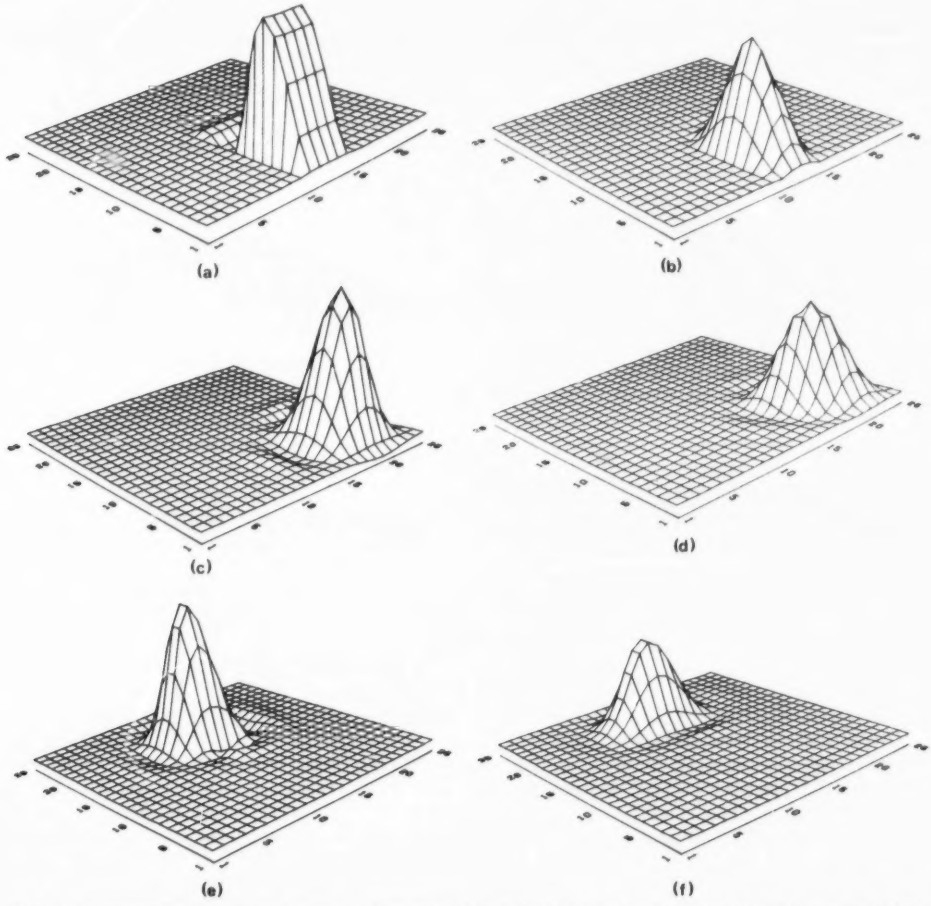

Fig. 5. Concentration fields of mass resulting from tests of the BIQUINTIC algorithm with (a) 1-D linear flow, block-shape initial mass, after 96 time steps, (b) 1-D linear flow, ellipse-shape initial mass, after 84 time steps, (c) 2-D linear flow, block-shape initial mass, after 96 time steps, (d) 2-D linear flow, ellipse-shape initial mass, after 84 time steps, (e) rotational flow, block-shape initial mass, afetr 300 time steps and (f) rotational flow, ellipse-shape initial mass, after 300 time steps.

both peaked distributions. The 2-D linear block test with this algorithm shows a mass (5c) with smoothly varying vertical cross-sections rather than rectangular ones, and the result of the ellipse test (5d) has preserved the integrity of the original shape considerably better than the other methods. Again, SHASTA-2 has greatly damped the peak concentration in both tests (4c and d), especially for the ellipse-shape, and flattened out the top of that distribution.

The results shown for the rotational tests have occurred after a time period more than three times longer into the simulations than in the linear advection tests. Thus distortion of the original shape might become more exaggerated here. For the block-shape, FCT4 and SHASTA-2 produced flat-top masses after one revolution (3e and 4e) and the BIQUINTIC test produced a very peaked mass with considerable negative rippling on all sides (5e). The SHASTA test has again greatly damped and diffused the original mass. Conversely, in the ellipse-tests the BIQUINTIC method maintained the original shape very well (5f), while FCT4 produced block-like distortions (3f) and SHASTA-2 nearly obliterated the original mass after 1 revolution (4f).

Time series of the mass distribution ratios for the tests provide a quantitative measure of the distortion in

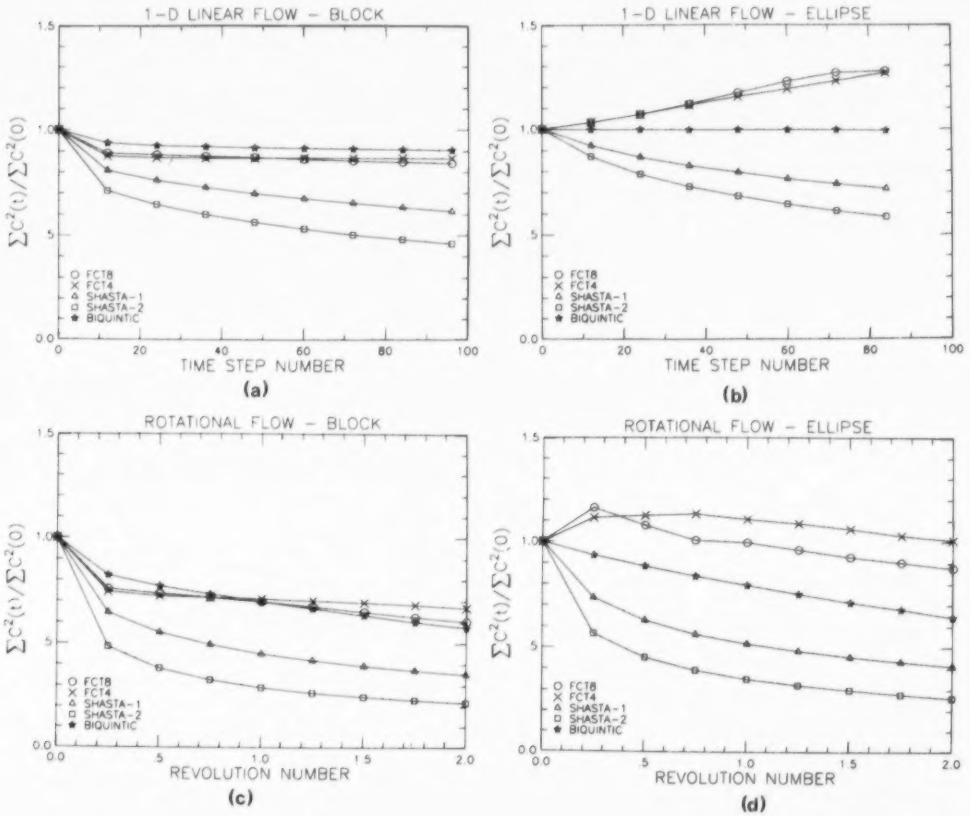

Fig. 6. Time series of the mass distribution ratios during the numerical simulations for (a) 1-D linear flow, block-shape initial mass, (b) 1-D linear flow, ellipse-shape initial mass, (c) rotational flow, block-shape initial mass and (d) rotational flow, ellipe-shape initial mass. For rotational flow, 1 revolution corresponds to 300 time steps.

Table 2. Summary of average absolute errors and execution times

Algorithm	Grand average absolute error	Average CPU time per numerical time step (s)	Accuracy–efficiency product (abs. error · CPU time)
FCT8	1.135	0.266	0.302
FCT4	1.093	0.224	0.245
SHASTA-1	2.130	0.082	0.175
SHASTA-2	2.124	0.099	0.210
BIQUINTIC	1.161	0.567	0.658

the shape of the original mass through the simulation. Ideally the ratio should be as close as possible to 1 at all times. Figure 6 displays this ratio for the 1-D linear and rotational flow tests. The BIQUINTIC algorithm produced results that were consistently closest to the original mass distributions in the 1-D linear tests. Moreover, the SHASTA schemes gave the lowest ratios in every case with the flux-corrected version, SHASTA-2, producing mass distribution ratios on the order of 0.5 toward the end of the simulations. The performance of the FCT methods were not as consistent. For the block tests (6a and c), both FCT8 and FCT4 gave results comparable to the BIQUINTIC method but in the ellipse cases (6b and d) the results diverge. The tendency for FCT methods to distort a peaked distribution toward a more block-like distribution, as discussed in the results shown in Fig. 5, can also produce a larger ratio. However, the opposite trend for the BIQUINTIC algorithm, as discussed previously, is not as easy to discern in the mass distribution ratios. It is hinted at in the rotational tests where the BIQUINTIC ratio drops somewhat faster in the block test (6c) than in the ellipse test (6d).

The time history of average absolute errors over the computational grid during the 1-D linear and rotational flow tests are shown in Fig. 7. It is not surprising that the smallest errors in the block tests are given by the FCT algorithms and the smallest errors in the ellipse tests by the BIQUINTIC method. The SHASTA techniques produced the largest average absolute errors in every case. Although not shown here, the trends in the maximum absolute errors over the grid follow those of the average absolute errors quite closely. The BIQUINTIC method again produces the smallest errors for the ellipse tests and the FCT schemes produce maximum errors that are larger than those of the other methods.

The points of consideration in the choice of a numerical advection algorithm should include not only the elements of accuracy but also the resources required to use the method. Typically the limiting resource factor is computer time. Table 2 presents the average computer (cpu) time per computational time step over all advection tests performed for each scheme. The average absolute error is also presented for each scheme over all tests as well as the product of these two parameters, a composite measure of the accuracy and efficiency of each method. A smaller value of this measure is a more desirable one. Both variations of the SHASTA technique are the fastest of the methods

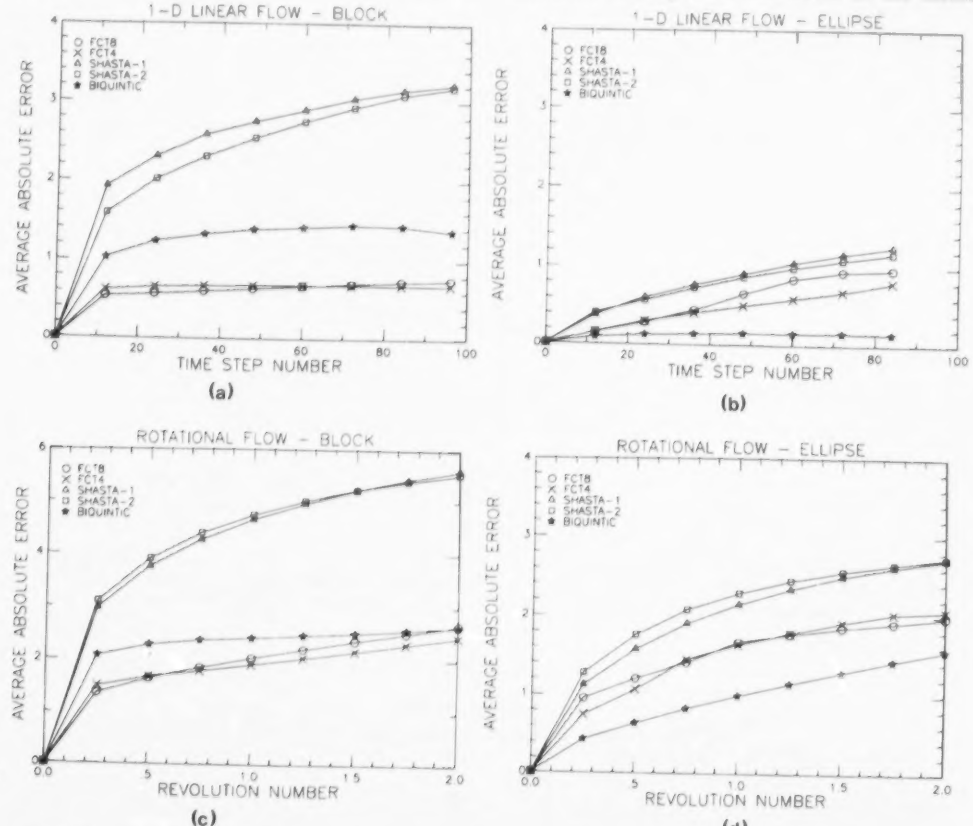

Fig. 7. Time series of the average absolute errors during the numerical simulations for (a) 1-D linear flow, block-shape initial mass, (b) 1-D linear flow, ellipse-shape initial mass, (c) rotational flow, block-shape initial mass and (d) rotational flow, ellipse-shape initial mass. For rotational flow, 1 revolution corresponds to 300 time steps.

tested here. Despite their higher average errors they still produce the smallest composite measures of accuracy and efficiency. However, the lower average errors for the FCT methods give them accuracy–efficiency products only slightly larger than the SHASTA techniques. Finally, the BIQUINTIC algorithm has an accuracy–efficiency product that is twice as high as any of the other schemes due solely to the longer computer time required.

5. CONCLUSIONS

Each of the numerical advection methods tested here has its own distinct advantages and drawbacks. All of the flux-corrected techniques, including SHASTA and FCT type methods, tend to distort a peaked distribution in the direction of a top-hat distribution. The superior accuracy–efficiency products of the SHASTA techniques are counterbalanced by the large amount of attendent numerical diffusion. In air quality simulation applications where the peak values are of greatest interest, the SHASTA method may not be adequate. A logical alternative lies in the FCT methods, which are multi-dimensional generalizations of SHASTA, do not require time-splitting in the solution process, and preserve the peak values in a mass distribution better than SHASTA does. The penalty for use of FCT is a longer execution time but its higher accuracy balances this cost.

Since the impetus for this study derived from the use of advection techniques in air quality simulation models, both the SHASTA and FCT methods were incorporated into the Urban Airshed Model for a test application. The resulting air quality concentration fields were very similar, except for larger values at the peaks and smaller values in the valleys with FCT. The relatively smooth gradients of mass in a simulation of actual urban ambient air quality compared to the more severe tests performed in this study mollified the differences between the two techniques. Also, the time penalty of FCT over SHASTA was reduced to 15% because of the other components of the model adding to the total time. The more accurate transport of the highest levels of concentration with the FCT methods verify that it is the more attractive algorithm in this application.

The relatively long execution time required for the BIQUINTIC algorithm apparently establishes it as the least attractive of the methods tested here. There are, however, many features of this technique that more than compensate for its longer execution time and may indeed prove the BIQUINTIC method to be preferable in many applications. As demonstrated here, it maintains the integrity of a peaked mass distribution better during transport than do the other methods tested. In an actual simulation of fluid flow there are other advantages. For one, it solves the diffusion component simultaneously with advection while most other techniques must do this in a separate step. It is also capable of solving a small portion of the computational grid at a time and is thus able to proceed by 'scrolling' the grid through the numerical solution and thereby saving a vast amount of computer storage. Lastly, and most significantly, the BIQUINTIC technique is independent of Courant number, which would otherwise dictate a prohibitively small time-step with the large grid cell dimensions in regional-scale air quality modeling work. It is entirely possible that the computer time requirements for this method will become more competitive with the others as vector machine techniques become more widespread.

This study has looked closely at a few selected methods for numerical advection as potential candidates for use in air quality models. There are many other methods and possible tests that exist that were not mentioned here. Further testing of these methods and use of various mass distributions in the tests is strongly encouraged.

Acknowledgements—The helpful discussions with Dr. Robert Lamb of EPA, Dr. Gregory McRae of Cal Tech and Dr. Nicholas Lordi of Form and Substance, Inc. were greatly appreciated.

REFERENCES

Book D. L., Boris J. P. and Hain K. (1975) Flux-corrected transport—II. Generalizations of the method. *J. Comput. Phys.* **18,** 248–283.

Boris J. P. and Book D. L. (1973) Flux-corrected transport—I. SHASTA, a fluid transport algorithm that works. *J. Comput. Phys.* **11,** 38–69.

Boris J. P. and Book D. L. (1976) Flux-corrected transport—III. Minimal-error FCT algorithms. *J. Comput. Phys.* **20,** 397–431.

Chock D. P. and Dunker A. M. (1983) A comparison of numerical methods for solving the advection equation. *Atmospheric Environment* **17,** 11–24.

Gentry R. A., Martin R. E. and Daly B. J. (1966) An Eulerian differencing method for unsteady compressible flow problems. *J. Comput. Phys.* **1,** 87–118.

Killus J. P., Meyer J. P., Durran D. R., Anderson G. E., Jerskey T. N. and Whitten G. Z. (1977) Continued research in mesoscale air pollution simulation modeling—Volume V. Refinements in numerical analysis, transport, chemistry and pollutant removal. Report ES77-142, Systems Applications, Inc., San Rafael, CA.

Lamb R. G. (1983) A regional scale (1000 km) model of photochemical air pollution. Part I—Theoretical formulation. EPA-600/3-83-035, Environmental Protection Agency, Research Triangle Park, NC.

Lamb R. G. and Mitchell C. (1983) Derivation of finite difference schemes using the Green's function of the differential equation. *J. Comput. Phys.* (submitted).

Reynolds S. D. and Roth P. M. (1983) The Systems Applications, Incorporated airshed model—a review and assessment of recent evaluation and applications experience. *J. Air Pollut. Control Ass.* (submitted)

Reynolds S. D., Roth P. M. and Seinfeld J. H. (1973) Mathematical modeling of photochemical air pollution—Part I. formulation of the model. *Atmospheric Environment* **7,** 1033–1061.

Roache P. J. (1972) *Computational Fluid Dynamics.* Hermosa Publishers, Albuquerque, NM.

Yanenko N. N. (1971) *The Method of Fractional Steps.* Springer, New York.

Zalesak S. T. (1979) Fully multidimensional flux-corrected transport algorithms for fluids. *J. Comput. Phys.* **31,** 335–362.